Desalination and Water Treatment
www.deswater.com

doi: 10.5004/dwt.2023.29234

284 (2023) 240–250
February

Photocatalytic degradation of Direct Red 80 using $ZnO/ZnTiO_3/Zn_2Ti_3O_8$ ternary nanocomposite

Kaveh Kalantari[a,*], Elham Asgari[b]

[a]*Department of Chemical Engineering, Faculty of Engineering, University of Zanjan, Zanjan, Iran, Tel. +98 24 3305 4064; email: k.kalantari@znu.ac.ir*
[b]*Department of Chemistry, Boroujerd Branch, Islamic Azad University, Boroujerd, Iran, email: e.asgari@iaub.ac.ir*

Received 26 July 2022; Accepted 19 December 2022

ABSTRACT

In the present study, novel zinc titanate-based nanocomposites were synthesized via an one-step sol–gel process. The crystalline structural, morphological and optical properties of the samples were characterized. Effect of Ti:Zn molar ratio on the structures and crystalline phase of the composites was investigated. $ZnO/ZnTiO_3/Zn_2Ti_3O_8$ ternary heterojunction catalyst obtained by Ti:Zn molar ratio of 1:1. The photocatalytic activity of the prepared nanocomposites with various Ti:Zn molar ratio was investigated for Direct Red 80 (DR80) degradation in aqueous solution. Excellent photocatalytic activity of $ZnO/ZnTiO_3/Zn_2Ti_3O_8$ nanocomposite exhibited 93.6% degradation of DR80 after 90 min irradiation which is 1.24 times of DR80 degradation using ZnO nanoparticles. The enhanced photocatalytic performance could be attributed to the formation of $ZnTiO_3$ as dominant phase and the heterojunction of electrons among $ZnTiO_3$, $Zn_2Ti_3O_8$ and ZnO, which enabled electron transfer in the nanocomposite, suppressed electron–hole pair recombination, and encouraged a wider light absorption by photocatalyst. The effect of main operating conditions on the photocatalytic degradation of dye was investigated using $ZnO/ZnTiO_3/Zn_2Ti_3O_8$ nanocomposite and optimum conditions were determined for degradation. The stability and cyclic efficiency of $ZnO/ZnTiO_3/Zn_2Ti_3O_8$ photocatalyst were investigated. Finally, the kinetic studies revealed the photocatalytic degradation kinetics of DR80 would follow a pseudo-second-order reaction.

Keywords: Zinc titanate; $ZnO/ZnTiO_3/Zn_2Ti_3O_8$ nanocomposite; Photocatalytic degradation; Direct Red 80 (DR80); Kinetic study

---

1. Introduction

Different industries, such as textiles, paper, leather, and food extensively use synthetic dyes. Their effluents cause serious threat to aquatic organisms and human beings when discharged into water bodies without appropriate treatment [1]. Therefore, decomposition of released dyes, especially azo dyes, in wastewater is necessary to avoid the dangers arising from their presence. Physical adsorption techniques, biological treatment methods and chemical methods are the mainly applied technologies for wastewater treatment. These traditional techniques are always not effective in dyes removing [2,3]. Accordingly, development of an economic, effective and eco-friendly wastewater treatment method has become a hot spot.

Recently, photocatalysis of organic pollutants as green chemistry process without secondary pollution has received great attention owing to its strong oxidation ability, simple and efficient operation and non-toxicity [4,5]. Among various semiconductors, TiO_2 and ZnO are greatly investigated as photocatalyst owing to their distinct advantages such as efficiency, high abundance, low-cost, non-toxicity and harmlessness [6–8]. However, some disadvantages such as excitation of electrons under UV light, wide band gap, high

---

[*] Corresponding author.

recombination rate of photo-excited electron–hole pairs and low stability of ZnO due to photo-corrosion restrict the application of pristine TiO_2 and ZnO [9,10]. Photocatalytic activity of ZnO and TiO_2 could be enhanced by improving photogenerated charges separation causes a high production of active species such as hydroxyl and superoxide radicals [11]. Various methods have been reported to efficiently separate the photogenerated electron–hole pairs, such as doping, metal loading, and introducing heterojunctions [12,13]. Among them, heterojunctions in photocatalysts has become a primary focus for researchers because of its possibility and efficiency in the separation of electron–hole pairs [14,15]. In heterojunction structures, recombination of photogenerated charges can be retarded by effective separation of electron–holes pairs, as well as the response range of light absorption can be broadened which results in increase the light-harvesting properties of photocatalyst [16,17]. Composite photocatalysts based on binary heterojunction of Ti and Zn compounds, such as TiO_2/ZnO, $ZnTiO_3$/TiO_2, ZnO/$ZnTiO_3$ etc., exhibit improved photocatalytic performance [18–21]. Das et al. [22] reported that TiO_2-ZnO nano-heterojunction with a suitable ratio of Ti:Zn can remarkably improve the photocatalytic performance than the pristine one owing to the effective charge carriers transfer across the interface. In spite of the improvement in photocatalytic efficiency of binary heterojunctions, some restrictions including undesirable separation of photogenerated charges and limited light response range can still be considered. Photocatalytic performance of composites can be further improved by constructing ternary heterojunction [23,24]. Zinc titanate consists three crystal phases: zinc metatitanate ($ZnTiO_3$), zinc polytitanate ($Zn_2Ti_3O_8$) and zinc orthotitanate (Zn_2TiO_4). The mentioned crystal phases can be converted to each other under some conditions [25]. $ZnTiO_3$ is an environmentally friendly compound for photocatalysis application [26]. The photocatalytic activity of perovskite $ZnTiO_3$ in the degradation of organic pollutants has been reported by several researchers [27,28]. $Zn_2Ti_3O_8$ as a metastable form of zinc titanate, can be considered as high potential material in photocatalytic reactions. So far, it is reported scarce researches concerning the synthesis, characterization and photocatalytic investigation of $Zn_2Ti_3O_8$. Pantoja-Espinoza et al. [29] reported the synthesis of $Zn_2Ti_3O_8$ and evaluated its photocatalytic activity in hydrogen production. Design of ternary zinc titanate-based composites can be an effective and feasible approach to achieve high-performance photocatalysts. There are few reports on ternary zinc titanate-based nanocomposites [30–32]. Yang et al. [30] reported the preparation of anatase-TiO_2/rutile-TiO_2/$ZnTiO_3$ heterojunction photocatalysts for hydrogen production. The separation of electron–hole pairs in this triphase photocatalyst might efficiently boost the photocatalytic activity. Yu et al. [31,32] synthesized Z-scheme $ZnTiO_3$/$Zn_2Ti_3O_8$/ZnO ternary heterojunction photocatalyst through a solvothermal-calcination route with suitable photocatalytic activity. The photocatalytic performance was ascribed to high separation efficiency of photogenerated charge carries via single Z-scheme.

Various multi-step synthesis processes have been utilized for preparation of ternary composites [33–35]. One-step synthesis process compared with multi-step synthesis has more important guiding significance for the formation of multi-component heterojunction [36]. Sol–gel synthesis method is noticed because of its advantages such as good uniformity of the structure, high purity, controllable and mild reaction conditions. In addition, sol–gel method is simple and has reproducible results [37]. In this study, novel zinc titanate-based nanocomposites, especially ZnO/$ZnTiO_3$/$Zn_2Ti_3O_8$ nanocomposites were synthesized via one-step sol–gel process. The effect of Ti:Zn molar ratio on the structure of synthesized composites was investigated. The crystalline structural, morphological and optical properties of the samples were characterized by means of X-ray diffraction (XRD), scanning electron microscopy (SEM), EDX and UV-Vis DRS measurements. Photocatalytic activity of the synthesized zinc titanate-based nanocomposites was investigated for degradation of Direct Red 80 (DR80) as an azo dye (Fig. 1). The effects of catalyst loading, pH and recycling of the photocatalyst on photodegradation performance were investigated. Furthermore, Kinetic studies were conducted. In order to compare the individual effect of pure ZnO and TiO_2 on the photocatalytic degradation of DR80 with the composites, pure ZnO and TiO_2 were synthesized by sol–gel method.

2. Experimental setup

2.1. Materials

Zinc acetate ($Zn(CH_3COO)_2 \cdot 2H_2O$) from Merck and titanium tetraisopropoxide (TTIP) from Sigma-Aldrich were used as zinc and titanium precursors, respectively. Isopropyl alcohol (IPA) and monoethanolamine (MEA) from Merck were used as solvent and stabilizer, respectively. All the chemicals were used without further purification.

2.2. Preparation of photocatalysts

The zinc titanate-based nanocomposites were prepared by sol–gel method. TTIP sol was prepared by adding TTIP to isopropyl alcohol with Ti:IPA molar ratio of 1:20 under magnet stirring. Then zinc acetate was gradually added to the solution with different molar ratios of Ti:Zn (2:1, 1:1, 1:2). The sol was stabilized by adding MEA and clear obtained solution was stirred for 1 h at 60°C. Deionized water was added to the solution. The molar ratio of MEA:(Ti+Zn) was

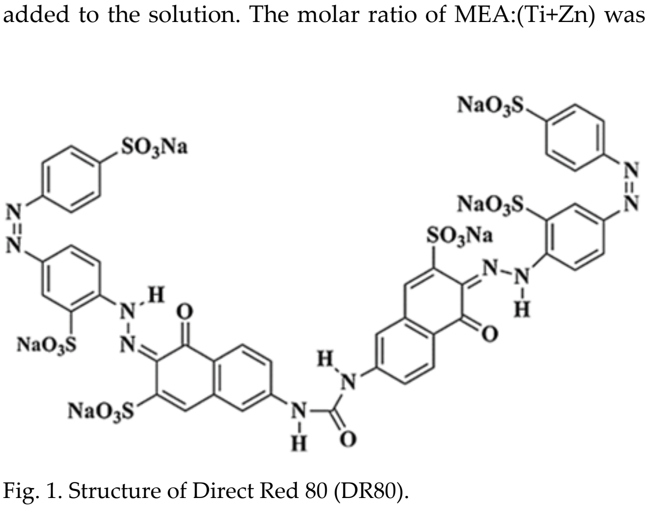

Fig. 1. Structure of Direct Red 80 (DR80).

optimized to be 2:1 in the preparation of all samples. All the sols were stable. The sols were aged at room temperature for 24 h. They were dried at 100°C for 1 h and then were calcined at 600°C for 1 h. The obtained nanocomposites were denoted as ZTN12, ZTN11 and ZTN21 for Ti:Zn molar ratios of 2:1, 1:1 and 1:2, respectively. Pure ZnO and TiO_2 nanoparticles were similarly synthesized. In order to synthesis ZnO nanoparticles, zinc acetate and MEA with Zn:MEA molar ratio of 2:1 was dissolved in appropriate amount of IPA. In order to synthesis TiO_2 nanoparticles, TTIP was dissolved in IPA under magnet stirring. Then MEA with Ti:MEA molar ratio of 1:1 was added. For both solutions, deionized water was added and the sols were continuously stirred at 60°C for 1 h to form clear solutions. The sols were separately aged at room temperature for 24 h. The products were dried and then calcined at 600°C for 1 h.

2.3. Characterization

The crystalline phases of prepared nanocomposites were investigated by XRD technique with a Bruker D8 advance X-Ray diffractometer. The morphological study of the samples was carried out using SEM technique with a Philips XL-30 scanning electron microscope. The chemical composition analysis was done by energy-dispersive X-ray spectroscopy (EDX) on a Vega electron microscope (Tescan Co.) equipped with a Rontec analyzer. The UV-vis diffuse reflectance spectroscopy (UV-Vis DRS) was conducted using a Cary-50 Scan UV-vis spectrophotometer (Varian, USA) for the optical characterization of photocatalysts.

2.4. Photocatalytic activity

The photocatalytic performance of the synthesized nanocomposites in DR80 degradation was investigated under ultraviolet (UV) light irradiation. Photocatalytic degradation of DR80 was conducted in a 100 mL pyrex reactor. The system was cooled using ventilation provided by fan inputting and removing air from the surface of the lamp and inside the reactor. A 65 W lamp was placed above the reactor as the UV light source. DR80 solution with a concentration of 15 mg/L was prepared as an initial solution. The experimental photocatalytic degradation of DR80 was carried out as follows. 25 mL of solution was placed in the reactor and the photocatalyst with appropriate loading concentration was added to the solution. The suspension was stirred in the dark for 1 h with magnetic stirrer to achieve adsorption–desorption equilibrium. Then the suspension was illuminated under constant stirring. During the light illumination, the samples were collected at selected time intervals and centrifuged to remove the photocatalysts. The concentration of DR80 was measured by monitoring absorption peaks with a UV-Vis spectrophotometer.

3. Results and discussion

3.1. Characterization

The XRD analysis is used to analyze the crystal structure, purity and crystallinity of the samples. Fig. 2a exhibits the XRD pattern of pure ZnO nanoparticles. The observed diffraction peaks may be ascribed to (100), (002), (101), (102), (110), (103), (200) and (112) crystal planes of wurtzite hexagonal crystal structure of the pure ZnO (JCPDS card No. 36-1451). The XRD pattern confirms the wurtzite structure of ZnO sample [38]. Determination of the exact source of some peaks (such as 2θ = 30.1°, 42.8° and etc.) in the obtained patterns is important. $Zn_2Ti_3O_8$ or Zn_2TiO_4 phases are likely to cause multiple peaks overlap at the mentioned 2θ [39]. On the other hand, structural similarity of $Zn_2Ti_3O_8$ to $ZnTiO_3$, as its metastable form, complicates phase determination due to nearness of the peaks 2θ positions [40]. It is reported that the cubic $Zn_2Ti_3O_8$ is a low temperature form of cubic $ZnTiO_3$ [41]. According to the reported studies on TiO_2-ZnO composites, formation of the cubic Zn_2TiO_4 spinel phase occurs at temperatures above 800°C [42]. Therefore, the mentioned peaks can be attributed to the $Zn_2Ti_3O_8$ phase (JCPDS NO.87-1781). Fig. 2b exhibits the XRD pattern of ZTN21 nanocomposite. The diffraction peaks at 2θ of 30°, 35.3°, 42.8° and 73.3° can be ascribed to the crystal planes of (220), (311), (400) and (533) of cubic $Zn_2Ti_3O_8$ spinel phase (JCPDS NO.87-1781), respectively. The observed peaks of 53°and 62° may be attributed to (205) and (214) crystal planes of hexagonal $ZnTiO_3$ phase (JCPDS NO.85-0547), respectively [43]. In addition, peaks corresponding to wurtzite ZnO are identified at 2θ of 31.8°, 34.5°, 36.3°, 47.6°, 56.6°, 63°, 66.4°, 68° and 69.2°. It can be attributed to the high ratio of Zn precursor to Ti precursor in the preparation stage. Absence of rutile and anatase phases demonstrates that all TiO_2 can be successfully converted into $ZnTiO_3$ and $Zn_2Ti_3O_8$ owing to the high amount of Zn. It can be seen that when the Ti:Zn molar ratio is 1:2, the $ZnO/ZnTiO_3/Zn_2Ti_3O_8$ heterojunction structures is formed and dominant phases are $Zn_2Ti_3O_8$ and ZnO. Fig. 2c shows the XRD pattern of ZTN11 nanocomposite. The diffraction peaks at 2θ of 30.1°, 42.8°, 53.5°, 55.9°, 57.2°, 62.5° and 73.5° belong to the crystal planes of (220), (400), (422), (510), (511), (440) and (533) of cubic $Zn_2Ti_3O_8$ phase, respectively (JCPDS NO.87-1781). The observed peaks of 35.4°, 53.1°, 56.9°, 62°, 63.4° and 74.4° may be attributed to (110), (205), (108), (214), (300) and (220) crystal planes of hexagonal $ZnTiO_3$ phase, respectively (JCPDS NO.85-0547) [26]. This figure also exhibits the existence of wurtzite ZnO at 2θ of 56.6° and 63°. According to the pattern, when the Ti:Zn ratio is 1:1, the $ZnO/ZnTiO_3/Zn_2Ti3O_8$ heterojunction structure is prepared with dominant phases of $ZnTiO_3$ and $Zn_2Ti_3O_8$. Therefore, this sample has relatively high purity of zinc titanate phases. Fig. 2d exhibits the XRD pattern of ZTN12 nanocomposite. When the Ti:Zn ratio increases to 2:1, the diffraction peaks become weak. ZTN12 sample has broader peaks than samples with lower Ti content, indicating the presence of smaller crystallites. The diffraction peaks at 2θ of 30.3° and 62.6° belong to the crystal planes of (220) and (440) of cubic $Zn_2Ti_3O_8$ spinel phase (JCPDS NO.87-1781), respectively. The peaks of 35.3°, 43.4° and 56.7° may be attributed to (110), (202) and (108) crystal planes of hexagonal $ZnTiO_3$ phase (JCPDS NO.85-0547) [39]. The diffraction peaks at 2θ of 27.5° and 41.4° may be attributed to (110) and (111) crystal planes of rutile TiO_2 (JCPDS NO.21-1276). The peaks of 38.7° and 53.9°may be indexed to (112) and (211) crystal planes of anatase TiO_2. (JCPDS NO.21-1272) [44]. The formation of rutile phase in TiO_2-ZnO composite with Ti:Zn molar ratio of 2:1 is reported at higher temperature

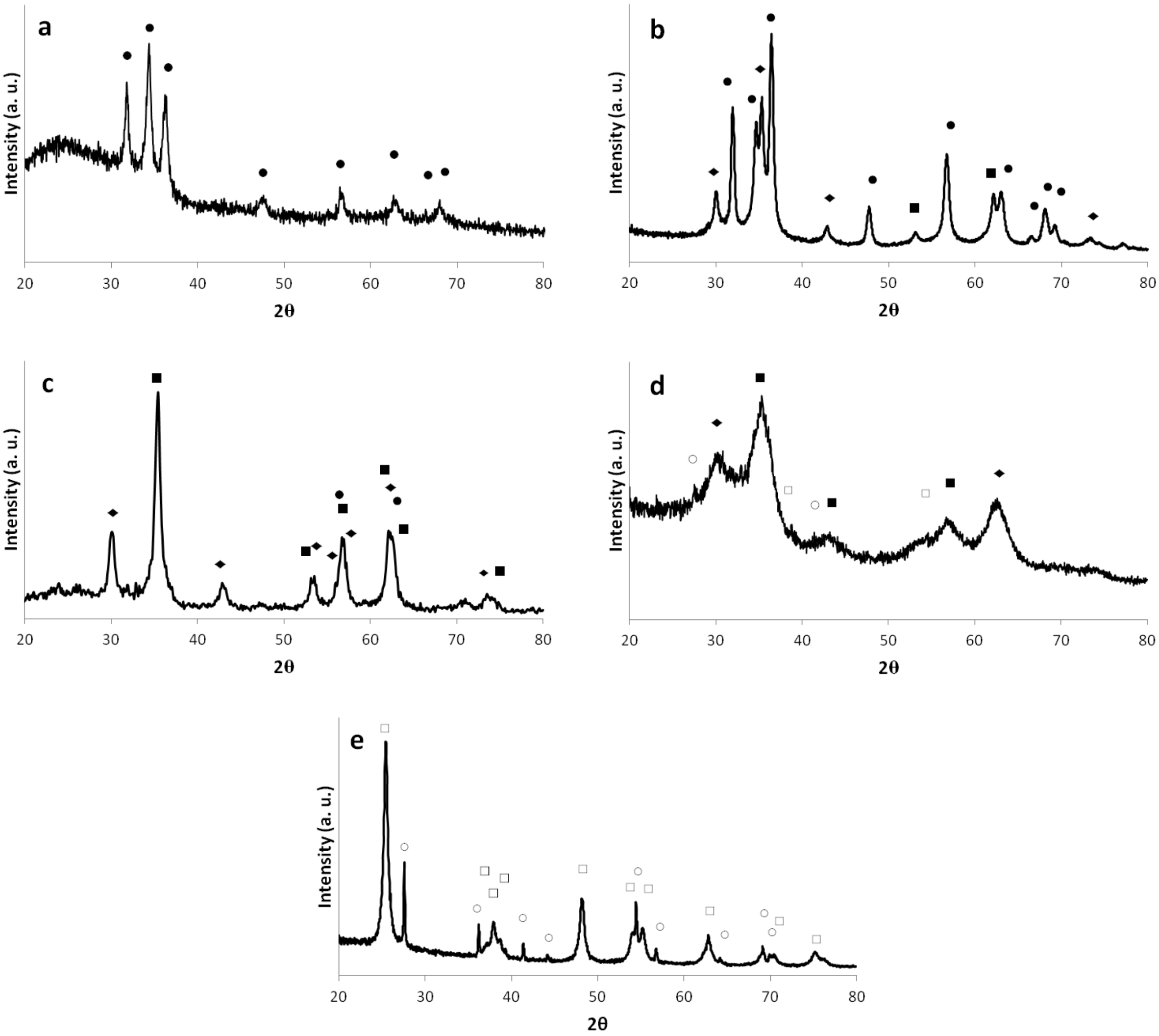

Fig. 2. XRD spectra of samples (a) ZnO, (b) ZTN21, (c) ZTN11, (d) ZTN12 and (e) TiO_2. (Peak identifications: (□) anatase, (○) rutile, (●) ZnO, (■) $ZnTiO_3$, and (♦) $Zn_2Ti_3O_8$).

(>700°) [43]. In this study rutile phase formed at 600°C. No peaks corresponding to ZnO was obtained in this sample. Immense amount of TiO_2 in the preparation stage leads to the presence of both anatase and rutile phases in addition to $ZnTiO_3$ and $Zn_2Ti_3O_8$ phases in the ZTN12 composite. Fig. 2e depicts XRD pattern of the pure TiO_2 nanoparticles. Both anatase and rutile phases exist in the sample while anatase is the major phase in this sample (JCPDS card No. 21-1272 and JCPDS card No. 21-1276) [45].

It can be concluded that the Ti:Zn molar ratio has great influence on the structure of the prepared samples. $ZnTiO_3$ formation occurs at 600°C which is much lower temperature than that suggested by earlier workers [46,47]. Formation of $ZnTiO_3$ and $Zn_2Ti_3O_8$ is observed in the ZTN21, ZTN11 and ZTN12 samples calcined at 600°C. TiO_2 reacts with ZnO along grain boundaries and forms $ZnTiO_3$ and $Zn_2Ti_3O_8$ phases [48]. Therefore, formation of heterojunction nanocomposites was confirmed by XRD results. When the XRD patterns of the synthesized composites are compared, it can be found out that the higher conversion of the precursor materials to the zinc titanate phases occurs in the equal molar ratio of Ti:Zn. The increase in the Ti:Zn molar ratio facilitates the formation of cubic $Zn_2Ti_3O_8$ in comparison with hexagonal $ZnTiO_3$ [49]. With increasing Zn content, the diffraction peaks become progressively intense. Formation of ZnO phase is boosted and wurtzite peaks become relatively more intense. High intensity peaks in the diffractograms of ZTN21 and ZTN11 reveal the presence of high crystalline phases. It is observed that the ZnO formation increases with a decrease in the molar ratio of Ti:Zn (ZTN12, ZTN11, ZTN21).

Fig. 3 exhibits the SEM images of the synthesized composites. Particles of the composites are granular and no variation in morphology is observed with increase the Ti:Zn ratio. The particle size of the synthesized composites with different Ti:Zn ratio ranges between 30–70 nm which confirms the formation of nanocomposites. SEM images also display the agglomeration of the nanoparticles. It seems that among of all the prepared nanocomposites, ZTN11 has the lowest agglomeration and ZTN12 has the highest agglomeration.

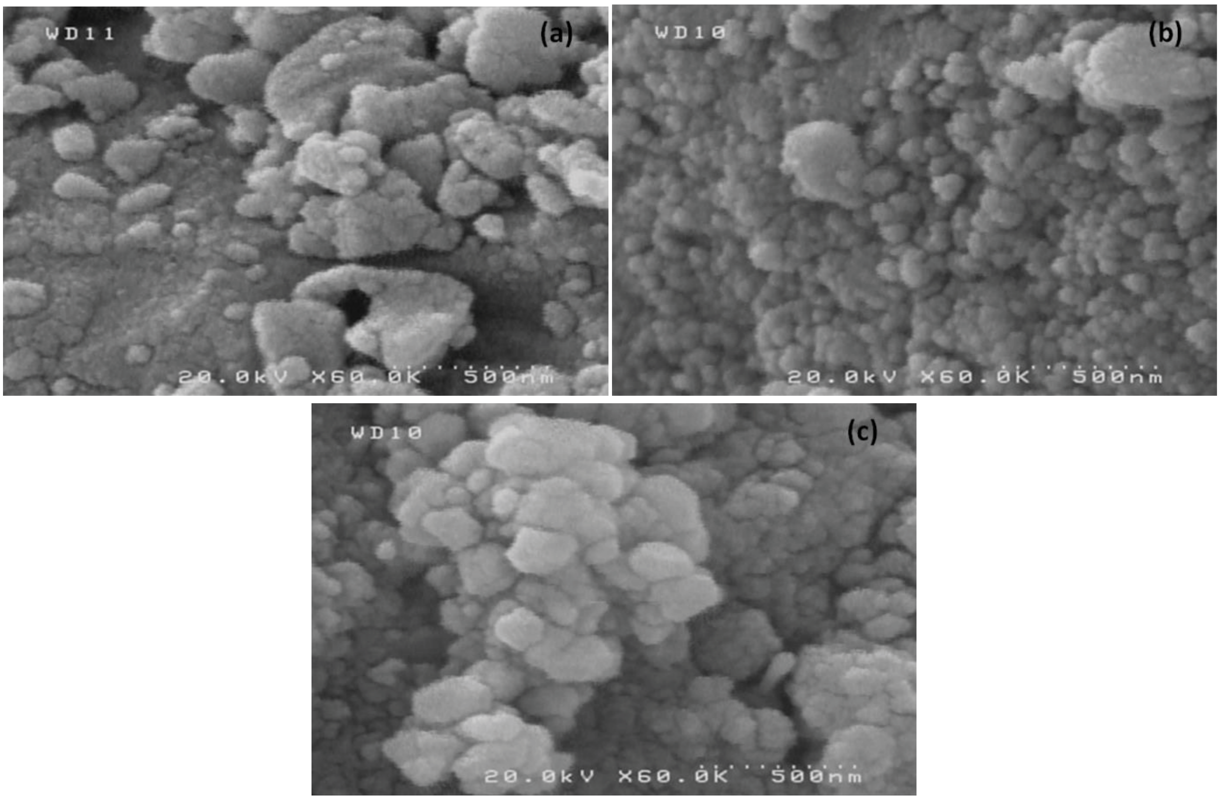

Fig. 3. SEM images of the samples: (a) ZTN21, (b) ZTN11 and (c) ZTN12.

Agglomeration in the nanoparticles affects on the specific surface area. Specific surface area is one of the parameters affecting on the heterogeneous photocatalysts activity by exposing photocatalytic active sites [50]. Lower agglomeration of the ZTN11 nanocomposite, compared to the other samples with different Ti:Zn ratio, can lead to a suitable catalytic activity of this sample.

In order to analyze the components of the nanocomposites, EDX analysis was performed. Fig. 4 illustrates the EDX spectra of the ZTN11 nanocomposite. Based on the EDX analysis, the nanocomposite is made of Ti, Zn and O elements and contains no impurities.

The optical properties of the ZTN11 sample were recorded as shown in Fig. 5. The UV-visible diffuse reflectance spectra of the nanocomposite are shown in Fig. 5a, which demonstrates the improved light absorption in the region of UV and visible light. The maximum absorption wavelengths of $ZnO/ZnTiO_3/Zn_2Ti_3O_8$ nanocomposite was about 420 nm and exhibited strong absorbance in the wavelength range of about 200–420 nm. The observed redshift in absorption edge of nanocomposite as compared to pure TiO_2 (365) and ZnO (391) [51] may be due to the differences in the surface state of the nanocomposite. The band gap energy of the ZTN11 nanocomposite can be calculated using the Kubelka–Munk function by plotting $(F(R)h\upsilon)^{1/2}$ vs. photon energy ($h\upsilon$) [52]. As shown in Fig. 5b, the extrapolation of the linear part of the spectrum to the photon energy axis determines the band gap energy of the sample. The band gap energy was calculated as 3 eV. It is reported that the band gap value of $ZnTiO_3$ is in the range of 3–3.2 eV [53,54]. The band gap value of the ZTN11 nanocomposite is close to the band gap value of $ZnTiO_3$ which can be corresponding to the presence of $ZnTiO_3$ as the major phase of nanocomposite. It can be noted that the presence of ZnO, $ZnTiO_3$ and $Zn_2Ti_3O_8$ in the ZTN11 nanocomposite can improve light absorption. The ZTN11 sample can be excited by lower energy, which improves the using efficiency of irradiation energy. Therefore, $ZnO/ZnTiO_3/Zn_2Ti_3O_8$ nanocomposite can more efficiently utilize light for the photocatalytic purpose due to light absorption ability in the higher wavelengths.

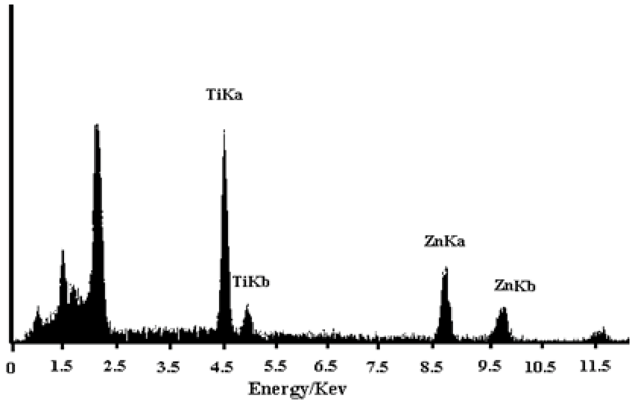

Fig. 4. EDX spectrum for the ZTN11 nanocomposite.

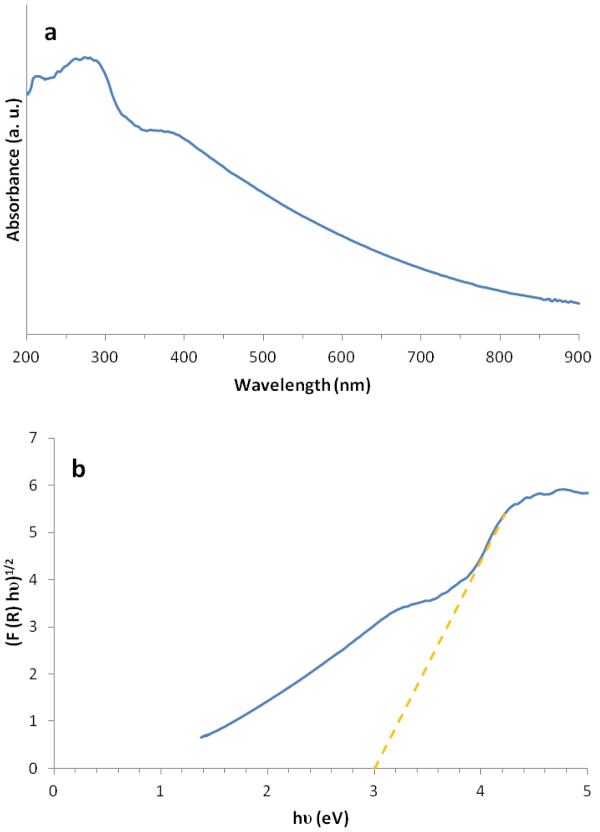

Fig. 5. (a) UV-Vis diffuse reflectance spectra of ZTN11 nanocomposite and (b) plot of the Kubelka–Munk function against the photon energy.

3.2. Photocatalytic activity

Photocatalytic degradation of DR80 was conducted under UV-light illumination to evaluate the photocatalytic activity of the synthesized nanocomposites, pure TiO_2 and ZnO nanoparticles. No DR80 was practically degraded in 90 min without using nanophotocatalysts or UV-light illumination, suggesting that DR80 is stable in the presence of nanophotocatalysts without light irradiation and no direct photolysis of the dye occurs under UV irradiation. It can be concluded that both nanophotocatalyst and light illumination are required for a significant degradation of DR80. Fig. 6 exhibits photocatalytic degradation of DR80 in the presence of different photocatalysts with catalyst loading of 3 g/L and pH-11 under UV irradiation. DR80 degradation is in the order of 93.6% (ZTN11) > 88.9% (ZTN21) > 82.7% (ZTN12) > 78.6% (TiO_2) > 75.5% (ZnO). It can be seen that DR80 degradation using nanocomposites is higher than that of the pure TiO_2 and ZnO nanoparticles. ZTN11 sample with $ZnO/ZnTiO_3/Zn_2Ti_3O_8$ ternary heterojunction structure exhibited the highest performance for DR80 degradation.

Type of the photocatalyst, crystallinity, size of the crystallites, surface area and agglomerations of particles are the factors affecting photocatalytic activity. The enhancement of photocatalytic activity of the nanocomposites in comparison with pure TiO_2 and ZnO may be attributed to the presence of the intimately bonded TiO_2/ZnO/zinc titanate surface heterostructure, which can enable a high charge carrier separation of the photogenerated electron–hole pair heterojunction and accordingly suppresses the recombination of electron–hole pairs. In addition, the XRD analysis results reveal the formation of Ti–O–Zn bonding for $ZnTiO_3$ and $Zn_2Ti_3O_8$ crystallites in the nanocomposites which could induce defects to the crystal lattice of TiO_2. These defects can lead to an increase in the absorption edge in comparison with the pure TiO_2 and ZnO. Based on the DRS analysis, the band gap energy of ZTN11 sample is obtained as 3 eV which is lower than that of pure TiO_2 and ZnO. Photogeneration of electron–hole pairs is boosted by increasing the light absorption which can improve the photocatalytic activity of the nanocomposites.

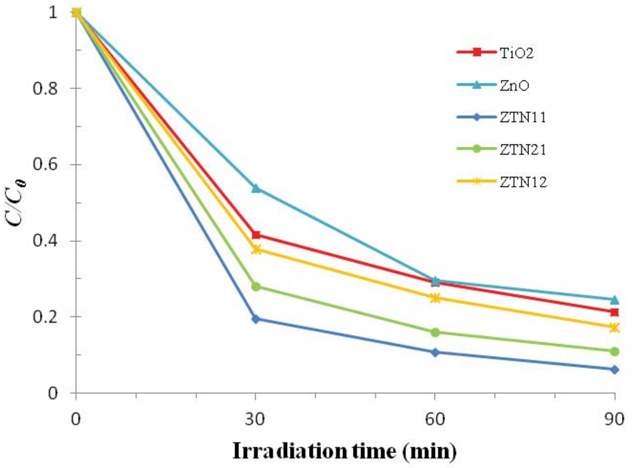

Fig. 6. Photocatalytic degradation of DR80 using different photocatalysts (photocatalyst loading: 3 g/L, pH-11).

The higher photocatalytic activity of ZTN21 and ZTN11 nanocomposites in comparison with ZTN12 sample may be due to the higher crystallinity and higher specific surface area of these samples. On the other hand, the presence of zinc oxide in ZTN21 and ZTN11 samples and titanium dioxide in ZTN12 sample can affect on their performance. As described previously, ZTN21 and ZTN11 nanocomposites comprise ZnO, $ZnTiO_3$ and $Zn_2Ti_3O_8$ and ZTN12 sample comprises TiO_2, $ZnTiO_3$ and $Zn_2Ti_3O_8$. The nature of the dominant phase can account for increase in photocatalytic activity. According to the XRD results, $ZnTiO_3$ phase is abundant in ZTN11 sample which is highly photoactive phase as reported by several researchers [27,55]. The band potentials of ZnO, $ZnTiO_3$ and $Zn_2Ti_3O_8$ in ZTN11 nanocomposite can form a ternary heterojunction facilitating the charge transfer and hinder the electron–hole recombination. Under UV light irradiation, electrons in the valence band (VB) are excited to conduction band (CB) resulting in generation of the same amount of holes in the VB. The photogenerated electrons and holes can be transferred among ZnO, $ZnTiO_3$ and $Zn_2Ti_3O_8$. The VB potentials of ZnO and $ZnTiO_3$ are more positive than that of $Zn_2Ti_3O_8$, resulting in the transfer of holes from the VB of ZnO and $ZnTiO_3$ to VB of $Zn_2Ti_3O_8$ across the interface of the heterostructures. Electrons can be transferred from $ZnTiO_3$ and $Zn_2Ti_3O_8$ to the surface of ZnO. This leads to the improved lifetime of charge carriers by hindering the electron–hole recombination. In this way the number of holes and electrons increases in the VB of $Zn_2Ti_3O_8$ and CB band of ZnO, respectively. The more numbers of electrons appear in the CB of ZnO can react with the surface oxygen molecules to produce highly reactive superoxide anion radicals ($^{\bullet}O^{-}_2$). On the other hand, the holes in the VB of $Zn_2Ti_3O_8$ can react with water molecules to produce hydroxyl radicals ($^{\bullet}OH$). The generated superoxide anion radicals and hydroxyl radicals can efficiently degrade the dye molecules [56,57]. Therefore, the efficient separation of electron–hole pairs and generation of active radicals can boost the photocatalytic activity of synthesized ZTN11 nanocomposite.

3.3. Effect of catalyst loading

Photocatalyst loading is one of the operating factors which has direct effect on the photodegradation rate in the photocatalytic processes [58]. The effect of photocatalyst loading was examined using ZTN11 nanocomposite ($ZnO/ZnTiO_3/Zn_2Ti3O_8$) with various catalyst loading ranging from 1–5 g/L. Maximum availability of the photocatalyst surface area and total absorption of incident light can be achieved by an optimum photocatalyst loading. Fig. 7 illustrates the photocatalytic degradation of DR80 in the presence of ZTN11 nanocomposite after 90 min under UV irradiation at pH-11. As shown in Fig. 7, degradation of DR80 increases as the nanocomposite loading is increased from 0 to 3 g/L. This may be attributed to the increased access of reactants and incident light to the catalyst surface area, which promotes the photocatalytic efficiency. At low photocatalyst loading, access of dye molecules to the photocatalyst active sites is limited due to the fewer number of existing active sites. Thus generation of active radicals is restricted by low photocatalyst loading. On the other hand, the light absorption by the photocatalyst reduces and photogeneration of electron–hole pairs are suppressed hence photocatalytic efficiency reduces. Therefore, photocatalytic degradation of DR80 enhances by increasing the photocatalyst loading. However, the dye degradation gradually decreases when the nanocomposite loading is increased from 3 to 5 g/L. High photocatalyst loading increases the turbidity of the reaction system, which leads to the light scattering and a diminution in the incident light penetration into the reaction system. Therefore, the light absorption on the photocatalyst surface is reduced leading to a decrease in photodegradation efficiency. On the other hand, presence of excess nanocomposites in the reaction system may lead to aggregation of its particles which causing the reduction of available surface area and consequently deactivation of photocatalyst [59]. Therefore, photocatalytic degradation of DR80 decreases slightly by further increasing the photocatalyst loading. The optimum ZTN11 nanocomposite loading is identified as 3 g/L.

3.4. Effect of pH

The pH of the reaction medium has an important role in the photocatalytic degradation of various pollutants in wastewater. The effect of the initial solution pH on the photocatalytic degradation of DR80 was investigated using the ZTN11 nanocomposite loading of 3 g/L in various pH values ranging from 7 to 11 under UV irradiation for 60 min. As shown in Fig. 8, degradation of DR80 boosts sharply as the pH value is increased from 7 to 11. The pH of the reaction medium could influence either the surface charge properties of the photocatalyst or the chemical forms of the intermediates, reactants or products. According to multiple roles of the pH parameter on the photocatalytic degradation of organic pollutants, explanation of its effect is difficult. On one hand, the pH could affect the ionization state of the photocatalyst surface and the ionic form of the organic compound. The electrostatic repulsion or attraction between the dye and photocatalyst surface could influence the adsorption of dye molecules onto the photocatalyst surface, as an important step for the photocatalytic degradation [60,61]. On the other hand, hydroxyl radicals have been observed to be formed by the reaction between hydroxide ions and positive holes. Positive holes are recognized as the major oxidizing species in the lower pH, while the hydroxyl radicals recognized as the

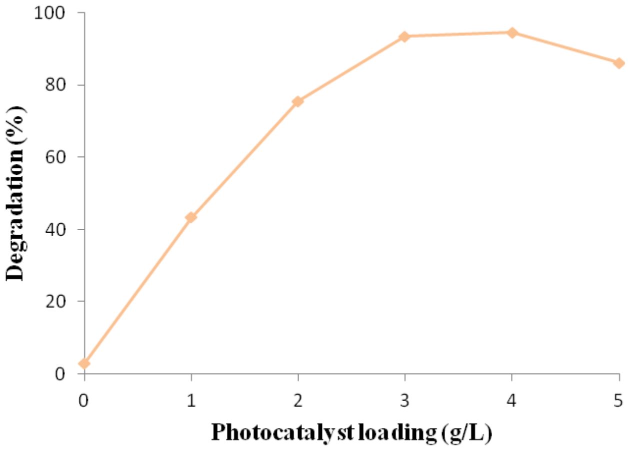

Fig. 7. Effect of ZTN11 photocatalyst loading on photocatalytic degradation of DR80.

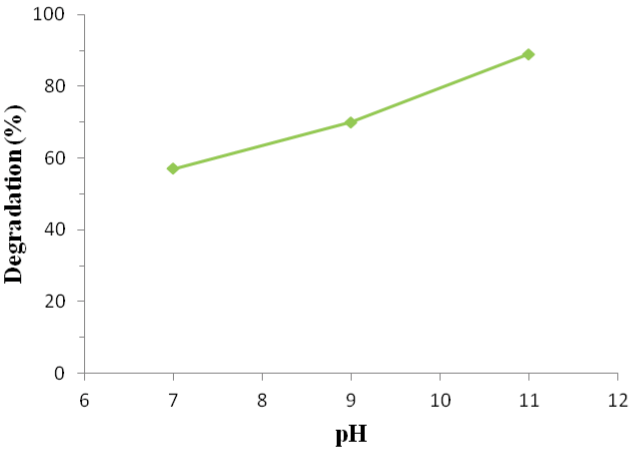

Fig. 8. Effect of reaction medium pH on photocatalytic degradation of DR80 using ZTN11 nanocomposite after 60 min irradiation (photocatalyst loading: 3 g/L).

dominant species in neutral or basic pH [62]. Generation of hydroxyl radicals is facilitated by oxidizing more hydroxide ions available on the surface of ZTN11 nanocomposite in basic solution leading to improve the photocatalytic process efficiency. However, in basic solution, the repulsion between the photocatalyst particles with negative charges and the hydroxide anions could suppress the generation of hydroxyl radicals and consequently decrease the photocatalytic process efficiency [63]. In this study, the increase of the degradation efficiency at the higher pH solution can be ascribed to the high hydroxylation of the ZTN11 nanocomposite surface owing to more available hydroxide ions. It can be noted that hydroxyl radicals seems to have a major role in DR80 dye degradation in comparison with photogenerated holes. Increasing the photodegradation efficiency in basic solution as shown in Fig. 8 is in agreement with previous works which elucidate that the highly basic pH facilitates photocatalysis [64,65].

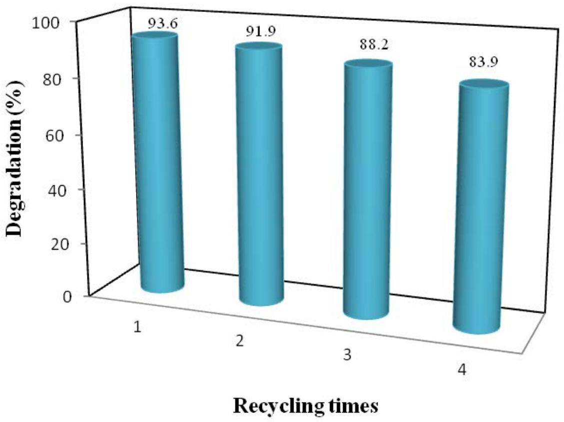

Fig. 9. Recycling activity of ZTN11 nanocomposite for DR80 degradation.

3.5. Effect of recycling of the photocatalyst

The reusability and stability of the ZTN11 nanocomposite was investigated by photocatalyst recycling. Photocatalytic degradation of DR80 repeated four times in similar operating condition using 3 g/L catalyst and 90 min irradiation. As shown in Fig. 9, a slight decrease in the DR80 degradation is observed. It can be deduced that the synthesized nanocomposite can maintain its photocatalytic efficiency for several reuses as an important factor in practical applications.

3.6. Kinetic model

Among many suggested kinetic models, pseudo-first-order and pseudo-second-order models have been extensively utilized in organic pollutants degradation studies [66–68]. The kinetic study for the photocatalytic degradation

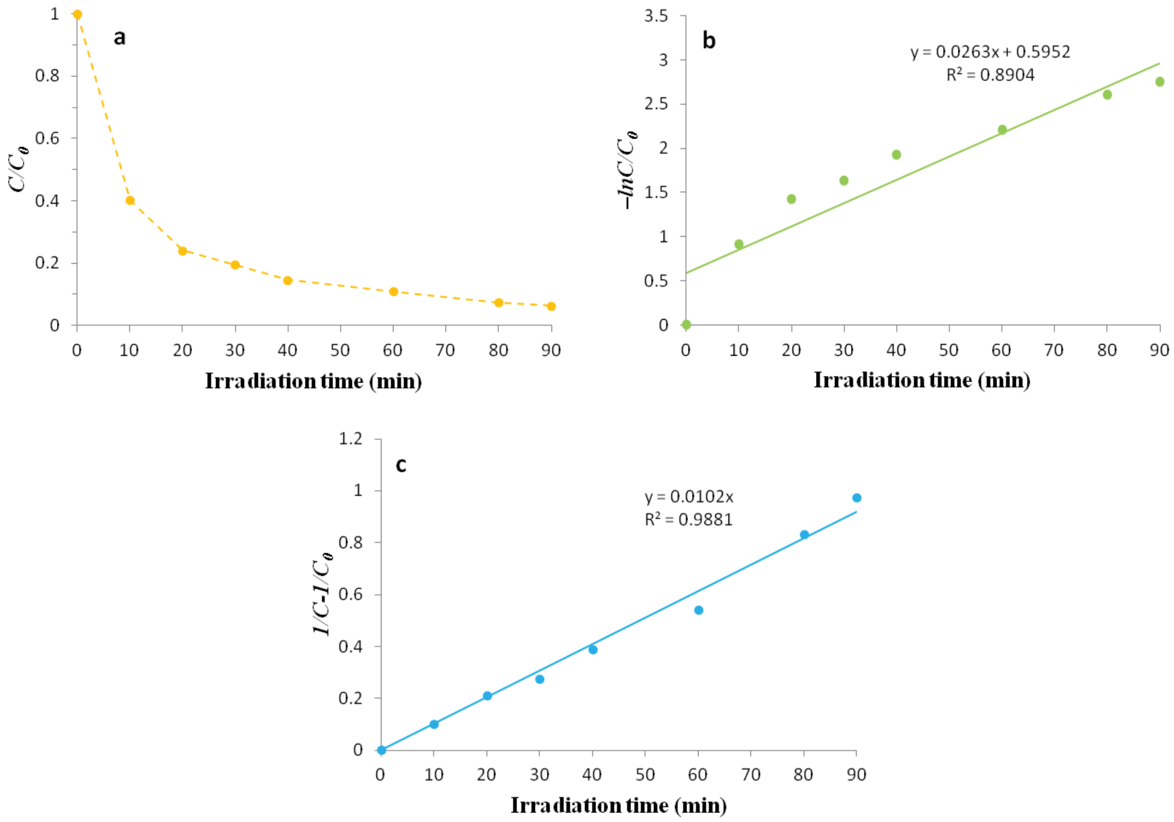

Fig. 10. (a) Photocatalytic degradation plot of DR80, (b) plot of pseudo-first-order kinetics for photocatalytic degradation of DR80, and (c) plot of pseudo-second-order kinetics for photocatalytic degradation of DR80.

of DR80 was investigated using pseudo-first-order and pseudo-second-order kinetic models. Fig. 10a presents the photocatalytic degradation plot of DR80 using $ZnO/ZnTiO_3/Zn_2Ti_3O_8$ nanocomposite, in which the operating condition of 3 g/L photocatalyst loading and pH-11(optimized operating conditions) were applied. Pseudo-first-order kinetics based on Langmuir–Hinshelwood kinetics when small initial concentration of the reactant is used can be described by Eq. (1)

$$-\ln\frac{C}{C_0} = k_1 t \tag{1}$$

where C_0 (mg/L) and C (mg/L) are DR80 concentrations at initial and reaction times, respectively, t is the irradiation time and k_1 is the apparent first-order rate constant of dye degradation. Fig. 10b depicts the plot of $-\ln C/C_0$ vs. time for $ZnO/ZnTiO_3/Zn_2Ti_3O_8$ nanocomposite within 90 min irradiation. The slope of the linear fitted plot depicts k_1 which was calculated as 0.026 min^{-1} and the coefficient of determination (R^2) was obtained as 0.89. Therefore, pseudo-first-order kinetic model showed an unsatisfactory quality of liner fitting.

Pseudo-second-order kinetic model can be described by Eq. (2):

$$\frac{1}{C_A} - \frac{1}{C_{A0}} = k_2 t \tag{2}$$

where k_2 (L/mg min) is the second-order kinetics rate constant and was determined from a linear fit to the data. Fig. 10c shows the plot of $(1/C-1/C_0)$ vs. t within 90 min irradiation. From the slope of the linear fitted plot the k_2 can be calculated as 0.01 L/mg min and the R^2 was obtained as 0.99. A much higher fitting quality is obtained by pseudo-second-order kinetics model equation. Based on these results, it can be concluded that the photodegradation of DR80 dye using $ZnO/ZnTiO_3/Zn_2Ti_3O_8$ nanocomposite follows pseudo-second-order reaction.

4. Conclusion

Zinc titanate-based nanocomposites were successfully prepared by one-step sol–gel method. Ti:Zn molar ratio controls the phase compositions and morphology of the heterojunction photocatalysts. Among the prepared nanocomposites, ZTN11 with $ZnO/ZnTiO_3/Zn_2Ti_3O_8$ ternary heterojunction structure (Ti:Zn molar ratio of 1:1) exhibited the highest performance for DR80 degradation. The enhancement of photocatalytic activity could be ascribed to the effective migration and separation of photo-generated electron–hole pairs, high crystallinity and morphology of $ZnO/ZnTiO_3/Zn_2Ti_3O_8$ nanocomposite. The optimum reaction conditions were determined as photocatalyst loading of 3 g/L and pH of 11. $ZnO/ZnTiO_3/Zn_2Ti_3O_8$ photocatalyst could be recycled and utilized several times with a slight decrease in the photocatalytic degradation efficiency. The photocatalytic degradation kinetics of DR80 by $ZnO/ZnTiO_3/Zn_2Ti_3O_8$ confirmed a pseudo-second-order reaction.

References

[1] T. Shindhal, P. Rakholiya, S. Varjani, A. Pandey, H.H. Ngo, W. Guo, H.Y. Ng, M.J. Taherzadeh, A critical review on advances in the practices and perspectives for the treatment of dye industry wastewater, Bioengineered, 12 (2021) 70–87.

[2] V. Selvaraj, T.S. Karthika, C. Mansiya, M. Alagar, An over review on recently developed techniques, mechanisms and intermediate involved in the advanced azo dye degradation for industrial applications, J. Mol. Struct., 1224 (2021) 129195, doi: 10.1016/j.molstruc.2020.129195.

[3] H.R. Dihom, M.M. Al-Shaibani, R.M.S.R. Mohamed, A.A. Al-Gheethi, A. Sharma, M.H.B. Khamidun, Photocatalytic degradation of disperse azo dyes in textile wastewater using green zinc oxide nanoparticles synthesized in plant extract: a critical review, J. Water Process Eng., 47 (2022) 102705, doi: 10.1016/j.jwpe.2022.102705.

[4] K. Kaur, R. Badru, P.P. Singh, S. Kaushal, Photodegradation of organic pollutants using heterojunctions: a review, J. Environ. Chem. Eng., 8 (2020) 103666, doi: 10.1016/j.jece.2020.103666.

[5] H. Dong, X. Zhang, H. Wu, C. Li, Nonmetal carbon-based photocatalysts for degradation of organic pollutants: a short review, Desal. Water Treat., 163 (2019) 260–269.

[6] M.H. Habibi, E. Askari, Synthesis of nanocrystalline zinc manganese oxide by thermal decomposition of new dinuclear manganese(III) precursors, J. Therm. Anal. Calorim., 111 (2013) 1345–1349.

[7] M.S. Çevika, Ö. Şahinb, O. Baytarb, S. Horozc, A. Ekincid, Investigation of the effect of magnesium and activated carbon on the photocatalytic degradation reaction of ZnO photocatalyst, Desal. Water Treat., 209 (2021) 212–218.

[8] Y. Xu, H. Wu, Z. Lv, Y. Cao, Synthesis of $Sr@TiO_2$ nanomaterials rapidly by microwave induced combustion method and measure its photocatalytic degradation properties of methyl orange wastewater, Desal. Water Treat., 245 (2022) 297–305.

[9] V. Vaiano, M. Matarangolo, J. Murcia, H. Rojas, J.A. Navío, M. Hidalgo, Enhanced photocatalytic removal of phenol from aqueous solutions using ZnO modified with Ag, Appl. Catal., B, 225 (2018) 197–206.

[10] X. He, A. Wang, P. Wu, S. Tang, Y. Zhang, L. Li, P. Ding, Photocatalytic degradation of microcystin-LR by modified TiO_2 photocatalysis: a review, Sci. Total Environ., 743 (2020) 140694, doi: 10.1016/j.scitotenv.2020.140694.

[11] S.G. Kumar, K.K. Rao, Comparison of modification strategies towards enhanced charge carrier separation and photocatalytic degradation activity of metal oxide semiconductors (TiO_2, WO_3 and ZnO), Appl. Surf. Sci., 391 (2017) 124–148.

[12] A. Shokri, M. Sanavi Fard, A critical review in the features and application of photocatalysts in wastewater treatment, Chem. Pap., 76 (2022) 5309–5339.

[13] C.-H. Wu, C.-Y. Kuo, C.-D. Dong, C.-W. Chen, Y.-L. Lin, Y.-S. Kuan, Synthesis, characterization, and photocatalytic activity of a novel Si_2O_3/Ag_3VO_4 heterojunction photocatalyst, Desal. Water Treat., 198 (2020) 364–375.

[14] J. Low, J. Yu, M. Jaroniec, S. Wageh, A.A. Al-Ghamdi, Heterojunction photocatalysts, Adv. Mater., 29 (2017) 1601694, doi: 10.1002/adma.201601694.

[15] X. Fang, J. Chen, J. Zhan, Heterojunction photocatalyst for organic degradation: superior photocatalytic activity through the phase and interface engineering, Ceram. Int., 46 (2020) 23245–23256.

[16] L. Zhu, H. Li, Q. Xu, D. Xiong, P. Xia, High-efficient separation of photoinduced carriers on double Z-scheme heterojunction for superior photocatalytic CO_2 reduction, J. Colloid Interface Sci., 564 (2020) 303–312.

[17] Ö. Tuna, E.B. Simsek, Construction of novel $Zn_2TiO_4/g\text{-}C_3N_4$ heterojunction with efficient photodegradation performance of tetracycline under visible light irradiation, Environ. Sci. Pollut. Res., 28 (2021) 10005–10017.

[18] H. Tian, S. Wang, C. Zhang, J.-P. Veder, J. Pan, M. Jaroniec, L. Wang, J. Liu, Design and synthesis of porous $ZnTiO_3/TiO_2$ nanocages with heterojunctions for enhanced photocatalytic H_2 production, J. Mater. Chem. A, 5 (2017) 11615–11622.

[19] R. Qin, F. Meng, M.W. Khan, B. Yu, H. Li, Z. Fan, J. Gong, Fabrication and enhanced photocatalytic property of TiO_2-ZnO composite photocatalysts, Mater. Lett., 240 (2019) 84–87.

[20] Q. Chen, L. Wu, X. Zhao, X.-J. Yang, Fabrication of Zn-Ti layered double oxide nanosheets with ZnO/$ZnTiO_3$ heterojunction for enhanced photocatalytic degradation of MO, RhB and MB, J. Mol. Liq., 353 (2022) 118794, doi: 10.1016/j.molliq.2022.118794.

[21] J.R. de Melo, D.M. de Oliveira, A.V. Scalco, A.M. Ferrari, N.R. Camargo Fernandes, M.L. Gimenes, Photocatalytic degradation of sulfonamide and its human metabolite by immobilized ZnO nanorods/TiO_2 nanoparticles, Desal. Water Treat., 256 (2022) 51–64.

[22] A. Das, P.M. Kumar, M. Bhagavathiachari, R.G. Nair, Hierarchical ZnO-TiO_2 nanoheterojunction: a strategy driven approach to boost the photocatalytic performance through the synergy of improved surface area and interfacial charge transport, Appl. Surf. Sci., 534 (2020) 147321, doi: 10.1016/j.apsusc.2020.147321.

[23] C.H. Nguyen, M.L. Tran, T.T. Van Tran, R.-S. Juang, Enhanced removal of various dyes from aqueous solutions by UV and simulated solar photocatalysis over TiO_2/ZnO/rGO composites, Sep. Purif. Technol., 232 (2020) 115962, doi: 10.1016/j.seppur.2019.115962.

[24] F. Wang, W. Li, S. Gu, H. Li, X. Liu, M. Wang, Fabrication of $FeWO_4$@$ZnWO_4$/ZnO heterojunction photocatalyst: synergistic effect of $ZnWO_4$/ZnO and $FeWO_4$@$ZnWO_4$/ZnO heterojunction structure on the enhancement of visible-light photocatalytic activity, ACS Sustainable Chem. Eng., 4 (2016) 6288–6298.

[25] C. Kang, K. Xiao, Z. Yao, Y. Wang, D. Huang, L. Zhu, F. Liu, T. Tian, Hydrothermal synthesis of graphene-$ZnTiO_3$ nanocomposites with enhanced photocatalytic activities, Res. Chem. Intermed., 44 (2018) 6621–6636.

[26] C. Chuaicham, S. Karthikeyan, J.T. Song, T. Ishihara, B. Ohtani, K. Sasaki, Importance of $ZnTiO_3$ phase in ZnTi-mixed metal oxide photocatalysts derived from layered double hydroxide, ACS Appl. Mater. Interfaces, 12 (2020) 9169–9180.

[27] S. Perween, A. Ranjan, Improved visible-light photocatalytic activity in $ZnTiO_3$ nanopowder prepared by sol-electrospinning, Sol. Energy Mater. Sol. Cells, 163 (2017) 148–156.

[28] R. Abirami, T. Senthil, S. Keerthana, R. Yuvakkumar, G. Ravi, M. Pannipara, A.G. Al-Sehemi, An approach to enhance the photocatalytic activity of $ZnTiO_3$, Ceram. Int., 47 (2021) 18122–18131.

[29] J.C. Pantoja-Espinoza, J.L. Domínguez-Arvizu, J.A. Jiménez-Miramontes, B.C. Hernández-Majalca, M.J. Meléndez-Zaragoza, J.M. Salinas-Gutiérrez, G.M. Herrera-Pérez, V.H. Collins-Martínez, A. López-Ortiz, Comparative study of $Zn_2Ti_3O_8$ and $ZnTiO_3$ photocatalytic properties for hydrogen production, Catalysts, 10 (2020) 1372, doi: 10.3390/catal10121372.

[30] Y. Yang, Y. Zhu, X. Ye, K. Zhou, P. Li, H. Chen, Y. Dan, W. Yang, H. Hou, One-dimensional mesoporous anatase-TiO_2/rutile-TiO_2/$ZnTiO_3$ triphase heterojunction with boosted photocatalytic hydrogen production activity, Catal. Lett., 151 (2021) 359–369.

[31] C. Yu, F. Chen, D. Zeng, Y. Xie, W. Zhou, Z. Liu, L. Wei, K. Yang, D. Li, A facile phase transformation strategy for fabrication of novel Z-scheme ternary heterojunctions with efficient photocatalytic properties, Nanoscale, 11 (2019) 7720–7733.

[32] F. Chen, C. Yu, L. Wei, Q. Fan, F. Ma, J. Zeng, J. Yi, K. Yang, H. Ji, Fabrication and characterization of $ZnTiO_3$/$Zn_2Ti_3O_8$/ZnO ternary photocatalyst for synergetic removal of aqueous organic pollutants and Cr(VI) ions, Sci. Total Environ., 706 (2020) 136026, doi: 10.1016/j.scitotenv.2019.136026.

[33] K.S. Ranjith, T. Uyar, ZnO-TiO_2 composites and ternary $ZnTiO_3$ electrospun nanofibers: the influence of annealing on the photocatalytic response and reusable functionality, CrystEngComm, 20 (2018) 5801–5813.

[34] M. Faisal, M. Jalalah, F.A. Harraz, A.M. El-Toni, J.P. Labis, M. Al-Assiri, A novel Ag/PANI/$ZnTiO_3$ ternary nanocomposite as a highly efficient visible-light-driven photocatalyst, Sep. Purif. Technol., 256 (2021) 117847, doi: 10.1016/j.seppur.2020.117847.

[35] H.S. Varaprasad, P. Sridevi, M.S. Anuradha, Optical, morphological, electrical properties of ZnO-TiO_2-SnO_2/CeO_2 semiconducting ternary nanocomposite, Adv. Powder Technol., 32 (2021) 1472–1480.

[36] J. Yao, Z. Gao, Q. Meng, G. He, H. Chen, One-step synthesis of reduced graphene oxide based ceric dioxide modified with cadmium sulfide (CeO_2/CdS/RGO) heterojunction with enhanced sunlight-driven photocatalytic activity, J. Colloid Interface Sci., 594 (2021) 621–634.

[37] U. Akpan, B. Hameed, The advancements in sol-gel method of doped-TiO_2 photocatalysts, Appl. Catal., A, 375 (2010) 1–11.

[38] K. Qi, X. Xing, A. Zada, M. Li, Q. Wang, S.-y. Liu, H. Lin, G. Wang, Transition metal doped ZnO nanoparticles with enhanced photocatalytic and antibacterial performances: experimental and DFT studies, Ceram. Int., 46 (2020) 1494–1502.

[39] J. Lu, D. Li, Y. Chai, L. Li, M. Li, Y. Zhang, J. Liang, Rational design and preparation of nanoheterostructures based on zinc titanate for solar-driven photocatalytic conversion of CO_2 to valuable fuels, Appl. Catal., B, 256 (2019) 117800, doi: 10.1016/j.apcatb.2019.117800.

[40] C.-T. Wang, J.-C. Lin, Surface nature of nanoparticle zinc-titanium oxide aerogel catalysts, Appl. Surf. Sci., 254 (2008) 4500–4507.

[41] P. Tahay, Y. Khani, M. Jabari, F. Bahadoran, N. Safari, A. Zamanian, Synthesis of cubic and hexagonal $ZnTiO_3$ as catalyst support in steam reforming of methanol: study of physical and chemical properties of copper catalysts on the H_2 and CO selectivity and coke formation, Int. J. Hydrogen Energy, 45 (2020) 9484–9495.

[42] L. Munguti, F. Dejene, Influence of annealing temperature on structural, optical and photocatalytic properties of ZnO-TiO_2 composites for application in dye removal in water, Nano-Struct. Nano-Objects, 24 (2020) 100594, doi: 10.1016/j.nanoso.2020.100594.

[43] N.T. Nolan, M.K. Seery, S.C. Pillai, Crystallization and phase-transition characteristics of sol-gel-synthesized zinc titanates, Chem. Mater., 23 (2011) 1496–1504.

[44] L. Ding, S. Yang, Z. Liang, X. Qian, X. Chen, H. Cui, J. Tian, TiO_2 nanobelts with anatase/rutile heterophase junctions for highly efficient photocatalytic overall water splitting, J. Colloid Interface Sci., 567 (2020) 181–189.

[45] K. Kalantari, M. Kalbasi, M. Sohrabi, S.J. Royaee, Enhancing the photocatalytic oxidation of dibenzothiophene using visible light responsive Fe and N co-doped TiO_2 nanoparticles, Ceram. Int., 43 (2017) 973–981.

[46] A. Sahu, R. Chaurashiya, K. Hiremath, A. Dixit, Nanostructured zinc titanate wide band gap semiconductor as a photoelectrode material for quantum dot sensitized solar cells, Sol. Energy, 163 (2018) 338–346.

[47] M. Salavati-Niasari, F. Soofivand, A. Sobhani-Nasab, M. Shakouri-Arani, A.Y. Faal, S. Bagheri, Synthesis, characterization, and morphological control of $ZnTiO_3$ nanoparticles through sol-gel processes and its photocatalyst application, Adv. Powder Technol., 27 (2016) 2066–2075.

[48] S. Jagtap, K. Priolkar, Evaluation of ZnO nanoparticles and study of ZnO-TiO_2 composites for lead free humidity sensors, Sens. Actuators, B, 183 (2013) 411–418.

[49] Z. Liu, D. Zhou, S. Gong, H. Li, Studies on a basic question of zinc titanates, J. Alloys Compd., 475 (2009) 840–845.

[50] K. Kalantari, M. Kalbasi, M. Sohrabi, S.J. Royaee, Synthesis and characterization of N-doped TiO_2 nanoparticles and their application in photocatalytic oxidation of dibenzothiophene under visible light, Ceram. Int., 42 (2016) 14834–14842.

[51] M.H. Habibi, M. Mikhak, Titania/zinc oxide nanocomposite coatings on glass or quartz substrate for photocatalytic degradation of direct blue 71, Appl. Surf. Sci., 258 (2012) 6745–6752.

[52] A. Murphy, Band-gap determination from diffuse reflectance measurements of semiconductor films, and application to photoelectrochemical water-splitting, Sol. Energy Mater. Sol. Cells, 91 (2007) 1326–1337.

[53] M. Sarkar, S. Sarkar, A. Biswas, S. De, P.R. Kumar, E.M. Mothi, A. Kathiravan, Zinc titanate nanomaterials–photocatalytic studies and sensitization of hydantoin derivatized porphyrin dye, Nano-Struct. Nano-Objects, 21 (2020) 100412, doi: 10.1016/j.nanoso.2019.100412.

[54] S. Lei, H. Fan, X. Ren, J. Fang, L. Ma, Z. Liu, Novel sintering and band gap engineering of $ZnTiO_3$ ceramics with excellent microwave dielectric properties, J. Mater. Chem. C, 5 (2017) 4040–4047.

[55] R. Abirami, C. Kalaiselvi, L. Kungumadevi, T. Senthil, M. Kang, Synthesis and characterization of $ZnTiO_3$ and Ag doped $ZnTiO_3$ perovskite nanoparticles and their enhanced photocatalytic and antibacterial activity, J. Solid State Chem., 281 (2020) 121019, doi: 10.1016/j.jssc.2019.121019.

[56] N. Sutanto, K.A. Saharudin, S. Sreekantan, V. Kumaravel, H. Md Akil, Heterojunction catalysts g-C_3N_4/-3ZnO-c-$Zn_2Ti_3O_8$ with highly enhanced visible-light-driven photocatalytic activity, J. Sol-Gel Sci. Technol., 93 (2020) 354–370.

[57] Y. Nosaka, A.Y. Nosaka, Generation and detection of reactive oxygen species in photocatalysis, Chem. Rev., 117 (2017) 11302–11336.

[58] S. Eydivand, M. Nikazar, Degradation of 1,2-dichloroethane in simulated wastewater solution: a comprehensive study by photocatalysis using TiO_2 and ZnO nanoparticles, Chem. Eng. Commun., 202 (2015) 102–111.

[59] D. Gupta, R. Chauhan, N. Kumar, V. Singh, V.C. Srivastava, P. Mohanty, T.K. Mandal, Enhancing photocatalytic degradation of quinoline by ZnO: TiO_2 mixed oxide: optimization of operating parameters and mechanistic study, J. Environ. Manage., 258 (2020) 110032, doi: 10.1016/j.jenvman.2019.110032.

[60] U.G. Akpan, B.H. Hameed, Parameters affecting the photocatalytic degradation of dyes using TiO_2-based photocatalysts: a review, J. Hazard. Mater., 170 (2009) 520–529.

[61] M.H. Habibi, E. Askari, The effect of operational parameters on the photocatalytic degradation of CI reactive yellow 86 textile dye using manganese zinc oxide nanocomposite thin films, J. Adv. Oxid. Technol., 14 (2011) 190–195.

[62] N.K. Nasab, Z. Sabouri, S. Ghazal, M. Darroudi, Green-based synthesis of mixed-phase silver nanoparticles as an effective photocatalyst and investigation of their antibacterial properties, J. Mol. Struct., 1203 (2020) 127411, doi: 10.1016/j.molstruc.2019.127411.

[63] S. Senobari, A. Nezamzadeh-Ejhieh, A comprehensive study on the enhanced photocatalytic activity of CuO-NiO nanoparticles: designing the experiments, J. Mol. Liq., 261 (2018) 208–217.

[64] A. Akbari, Z. Sabouri, H.A. Hosseini, A. Hashemzadeh, M. Khatami, M. Darroudi, Effect of nickel oxide nanoparticles as a photocatalyst in dyes degradation and evaluation of effective parameters in their removal from aqueous environments, Inorg. Chem. Commun., 115 (2020) 107867, doi: 10.1016/j.inoche.2020.107867.

[65] X.-H. Ou, C.-H. Wu, S.-L. Lo, Photodegradation of 4-chlorophenol by UV/photocatalysts: the effect of the interparticle electron transfer process, React. Kinet. Catal. Lett., 88 (2006) 89–95.

[66] W. Gao, C. Ran, M. Wang, L. Li, Z. Sun, X. Yao, The role of reduction extent of graphene oxide in the photocatalytic performance of Ag/AgX (X = Cl, Br)/rGO composites and the pseudo-second-order kinetics reaction nature of the Ag/AgBr system, Phys. Chem. Chem. Phys., 18 (2016) 18219–18226.

[67] Z. Li, X. Chen, M. Wang, X. Zhang, L. Liao, T. Fang, B. Li, Photocatalytic degradation of Congo red by using the Cu_2O/alpha-Fe_2O_3 composite catalyst, Desal. Water Treat., 215 (2021) 222–231.

[68] A. Ghenaatgar, R.M. Tehrani, A. Khadir, Photocatalytic degradation and mineralization of dexamethasone using WO_3 and ZrO_2 nanoparticles: optimization of operational parameters and kinetic studies, J. Water Process Eng., 32 (2019) 100969, doi: 10.1016/j.jwpe.2019.100969.